

# Polymer Chemistry

Accepted Manuscript



This is an *Accepted Manuscript*, which has been through the Royal Society of Chemistry peer review process and has been accepted for publication.

*Accepted Manuscripts* are published online shortly after acceptance, before technical editing, formatting and proof reading. Using this free service, authors can make their results available to the community, in citable form, before we publish the edited article. We will replace this *Accepted Manuscript* with the edited and formatted *Advance Article* as soon as it is available.

You can find more information about *Accepted Manuscripts* in the [Information for Authors](#).

Please note that technical editing may introduce minor changes to the text and/or graphics, which may alter content. The journal's standard [Terms & Conditions](#) and the [Ethical guidelines](#) still apply. In no event shall the Royal Society of Chemistry be held responsible for any errors or omissions in this *Accepted Manuscript* or any consequences arising from the use of any information it contains.

Cite this: DOI: 10.1039/coxx00000x

www.rsc.org/xxxxxx

ARTICLE TYPE

# Large-scale synthesis of organometallic polymer flowers with ultrathin petals for hydrogen peroxide sensing†

Guodong Liang,\* Xiaodong Li, Suping Bao, Haiyang Gao, Fangming Zhu and Qing Wu

*Received (in XXX, XXX) Xth XXXXXXXXXX 20XX, Accepted Xth XXXXXXXXXX 20XX*

DOI: 10.1039/b000000x

Functional nanostructures are crucial for fabrication of nanodevices in the future. Herein we reported a facile and efficient approach for large-scale synthesis of organometallic polymer flowers. This approach involved crystallization of polyethylene (PE) capped with cyanoferrate complex in the presence of polymeric dispersants, and subsequent *in situ* coordination polymerization of cyanoferrate complex with  $\text{Fe}^{3+}$ . This afforded polyethylene/Prussian blue (PE-PB) hybrid flowers with ultrathin petals of 7 nm, in which PE lamellae were sandwiched between two PB nanolayers. Morphological analysis revealed that the addition of proper amount of hydrophobic poly(propylene glycol) favoured the formation of hybrid flowers. PE-PB flowers synthesized showed enhanced surface area and improved electrocatalytic activity towards reduction of hydrogen peroxide. Such crystallization induced flowers of organometallic polymers offer a class of functional nanomaterials, which are useful for biosensing and nanodevices.

## Introduction

Nanomaterials based on organometallic polymers have attracted increasing attention because of large surface area offering them a broad range of potential applications in sensing, catalysis, gas storage, and so on.<sup>1-7</sup> Controlling morphologies of the nanomaterials has been proved to be a promising approach for optimizing their properties and exploring new functionalities. In particular, flower-like nanomaterials have received numerous interests due to their overwhelming advantages such as immunity to aggregation, large surface area, low packing density, light weight, and so on. Inorganic flowers including metals and metal oxides using electrodeposition or wet chemistry approaches have been intensively investigated, which show enhanced magnetic, catalytic, self-cleaning performances.<sup>8-16</sup> Recently, polymer flowers exhibiting superior hydrophobicity have also been achieved by self-assembly of polymers.<sup>17, 18</sup> On the other hand, hybrid flowers containing both functional metal species and polymers are considered to be promising materials, which inherit the advantages of their parent components and generate new functions to meet demands in engineering sectors. In this respect, difficulties lie in structure control of multi-components at nanoscale, which are chemically distinct and immiscible. This makes the synthesis of hybrid flowers remain challenging.

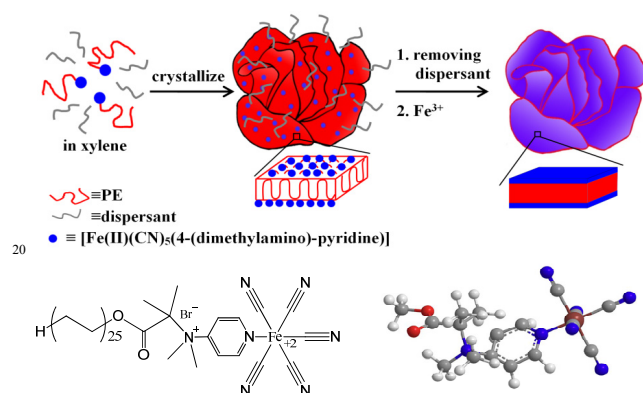
Crystallization is recognized as one of driving forces for the formation of polymeric nanostructures recently. Macromolecular chains fold back and forth during crystallization to form anisotropic nanostructures with varied morphologies including rods, lamellae, and so on, depending on the composition and chain structure of polymers as well as self-assembly conditions.<sup>19-24</sup> PFS based copolymers (PFS: poly(ferrocenyldimethylsilane)) self assembled into cylindrical micelles with PFS forming cores surrounded by a corona of the other blocks, which was driven by

crystallization of PFS block. The cylinders were capable of acting as seeds and growing in a living manner when more copolymers were added.<sup>25-28</sup> Crystallization-driven cylindrical micelles were amendable to PE (polyethylene) and PCL (poly( $\epsilon$ -caprolactone)) based block copolymers.<sup>29-31</sup>

Previously, we synthesized polyethylene/Prussian blue hybrid flowers by crystallization assisted interface coordination polymerization (CAICP).<sup>32</sup> Polyethylene terminated with cyanoferrate complex (PE-Fe) was allowed to crystallize in diluted solution. During crystallization of polymers, cyanoferrate complex was expelled out of polymer crystal lamellae, and finally located on the surface.<sup>21</sup> Such inorganic ferrate layer having high free energy was inclined to initiate crystallization of macromolecules in turn, which led to the formation of perpendicularly-stacked lamellae. When the rate of crystal growth and nucleation were comparable, flower-like particles formed. Subsequent coordination polymerization of cyanoferrate complex with  $\text{Fe}^{3+}$  on surface resulted in polyethylene/Prussian blue (PE-PB) hybrid flowers. We demonstrated that only in diluted solution, *i.e.* 0.1 mg/mL, well-defined flowers with thin petals formed. The low concentration used in synthesis procedure makes mass-production of PE-PB flowers difficult. For instance, to synthesize 1.0 g PE-PB flowers, bulky volume of solvents (10 litres of xylene) is required. This causes increased costs, low efficiency, environmental issues and difficulties in isolation of products. This strictly limits their applications in engineering sectors. Thus, developing new approaches for large-scale synthesis of hybrid flower-like nanomaterials is highly desirable.

Herein, we reported a facile approach for large-scale synthesis of organometallic polymer flowers. Crystalline polyethylene terminated with cyanoferrate complex (PE-Fe) was allowed to crystallize in concentrated solution (2.0 mg/mL). To

offset the increased crystal growth rate caused by high concentration, we introduced polymeric dispersants to inhibit crystal growth. We demonstrated that the increased crystal growth rate could be offset by introducing proper dispersants. Consequently, well-defined flower-like particles with thin petals were achieved even in concentrated solution (Scheme 1). This significantly decreases the amount of solvents used (1/20 of that without dispersants), and promises mass-production of hybrid flowers. PE-PB hybrid flowers synthesized showed an enhanced surface area and improved electrocatalytic activity and stability towards reduction of hydrogen peroxide. While polymer/PB hybrid nanoparticles with varied morphologies including nanoshells, nanocubes, vesicles, nanoribbons have been reported,<sup>33-45</sup> the large-scale synthesis of polymer/PB hybrid flowers is unprecedented to our best knowledge. Such crystallization driven nanostructures offer a class of new functional nanomaterials useful for bio-sensing, nano-devices, and so on.



**Scheme 1** Schematic illustration for large-scale synthesis of PE-PB hybrid flowers in the presence of polymeric dispersants, chemical structure and ball-stick modelling of polyethylene terminated with [Fe(II)(CN)<sub>5</sub>(4-(dimethylamino)-pyridine)] (PE-Fe). For clarity, methyl group was used to stand for polyethylene in the ball-stick modelling.

## Results and discussion

### Synthesis of PE-PB flowers

The organometallic PE-PB polymer was analyzed by using FT-IR, Raman and XPS measurements. In FT-IR spectra (Fig. 1A), an absorbance band at 2060 cm<sup>-1</sup> was observed for PE-Fe, attributed to C≡N stretching vibration. This band blue-shifted to 2084 cm<sup>-1</sup> after coordination polymerization due to the formation of Fe(II)-CN-Fe(III) bridge in PE-PB composites.<sup>46</sup> Raman spectra showed that the peak at 2100 cm<sup>-1</sup> attributed to C≡N stretching vibration of PE-Fe,<sup>47</sup> blue-shifted to 2154 cm<sup>-1</sup> for PE-PB flowers (Fig. 1B), consistent with the FT-IR results.

The chemical composition of PE-PB flowers was analyzed using X-ray photoelectron spectroscopy (XPS) as shown in Fig. 2. The XPS survey spectrum of PE-PB flowers showed the presence of Fe element originating from Prussian blue, O and Br elements from the polymers, C and N elements from PB and polymers. Fe2p pattern revealed the levels of Fe2p<sub>3/2</sub> located at 708.4 eV, stemming from Fe(II) of PB. Moreover, the peaks at 711.8 eV

and 721.4 eV, attributed to Fe2p<sub>3/2</sub> and Fe2p<sub>1/2</sub>, respectively, of Fe(III) of PB were also observed. The C1s spectrum of PE-PB flowers showed the peaks at 285, 285.7, 296.5 and 289 eV, ascribed to C-C, C-N, C-O and carboxyl groups, respectively. The C-N peak at 285.7 eV further confirmed the presence of ferrate complex in the hybrid flowers.<sup>48, 49</sup>

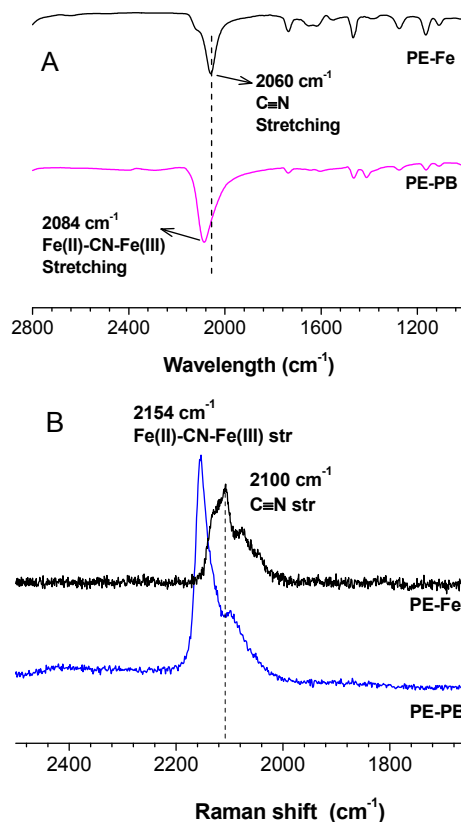


**Fig. 1** (A) FT-IR spectra and (B) Raman spectra for PE-PB flowers and PE-Fe.

### Morphology of PE-PB flowers

Morphology of PE-PB hybrid flowers was characterized using field-emission scanning electron microscopy (SEM) (Fig. 3). A typical SEM image illustrated that PE-PB flowers had a diameter of ca. 3 μm. SEM images at higher magnifications showed that the flowers possessed ultrathin petals. Thickness of petals of flowers was determined to be approximately 7 nm from the standing petals, close to the fully extended chain length of PE-Fe (supporting information, Scheme S1), implying that the petals consisted of a single PE layer. Moreover, no obvious ordered structures were observed at the rim of flower petals in TEM images at high magnitudes (Fig. 3D), suggesting that PB was amorphous in PE-PB flowers. Polyethylene (PE) segments exist as random coils in xylene at 120 °C. When temperature cools down, PE chains fold back and forth to form lamellae, regarded as crystallization. During crystallization of PE, end groups of ferrate complex are expelled out of lamellae and reside on the surface. Such inorganic ferrate layers having high free energy are inclined to absorb PE segments and initiate crystallization of PE in turn. When the crystallization growth rate and nucleation rate are comparable, flower-like structures form.<sup>32</sup>

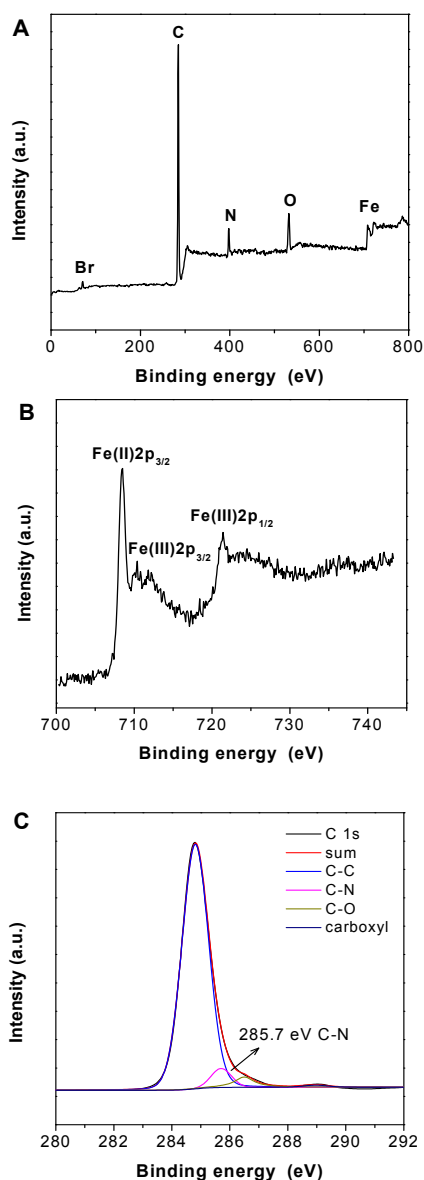


**Fig. 2** (A) Survey spectrum, (B) Fe 2p XPS pattern and (C) C 1s XPS spectrum of PE-PB flowers.

### Effect of poly(propylene oxide) (PPO) fractions

Concentrated PE-Fe/xylene solution (*i. e.* 2 mg/mL) was not stable. Upon cooling from 120 °C to low temperature (*i. e.* 46 °C), polymers precipitated and formed large aggregates due to rapid crystallization of PE-Fe. In contrast, in the presence of the equivalent weight of poly(propylene oxide) (PPO), PE-Fe suspension was stable over 2 days upon cooling to a low temperature. Thus, we investigated the effect of PPO fractions on morphology of PE-PB particles. In the absence of PPO, large aggregate formed (Fig. S1). Flower-like structures with thick petals were obtained at PPO/PE-Fe weight ratio of 0.2:1. Increasing PPO/PE-Fe weight ratio to 0.5:1 gave rise to flower-like structures together with a few large aggregates. Further increasing PPO/PE-Fe weight ratio to 2:1, irregular aggregates were observed. This revealed that optimized PPO/PE-Fe ratio of

1:1 existed for the formation of PE-PB flowers.

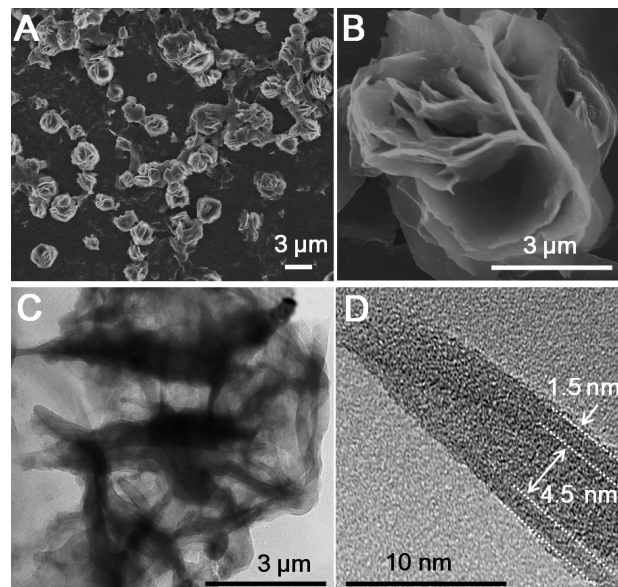


**Fig. 3** Scanning electron microscopy (SEM) images (A) at low magnification and (B) at high magnification, as well as transmission electron microscopy (TEM) images (C) at low magnification and (D) at high magnification of PE-PB hybrid flowers.

We monitored crystallization of PE-Fe in the presence and absence of PPO using differential scanning calorimetry (DSC), as shown in Fig. 4. Distinct exotherm observed for both PE-Fe and PE-Fe/PPO indicated that crystallization of PE occurred. PE-Fe/PPO showed a broader exothermic peak in contrast to PE-Fe, which indicated that it took longer time for PE-Fe to crystallize in the presence of PPO. Crystallization half-time for PE-Fe/PPO was determined to be 0.45 min, double of that for PE-Fe in the absence of PPO (0.21 min). While the crystallization rate constant for PE-Fe/PPO was half of that for PE-Fe (supporting information, Fig. S2 and Table S1). This demonstrated that crystallization of PE-Fe was slowed down in the presence of PPO. In the subsequent heating scan, PE-Fe and PE-Fe/PPO showed an endothermic peak, which further confirmed crystallization of PE. The degree of crystallinity of PE-Fe in the presence and absence of PPO was close to each other (36.7% and 38.5%, respectively), although PE-Fe/PPO mixture exhibited broader endotherm than PE-Fe. This implied that PPO hindered, but did not suppress crystallization of PE-Fe. In the absence of PPO, when PE-Fe crystallizes from the concentrated solution (*i. e.* 2 mg/mL), its crystal growth rate is high due to quick diffusion of uncrystalline segments towards crystalline sites. Therefore, large aggregates form. In the presence of PPO, PE-Fe macromolecules are isolated by PPO chains, which prevent PE-Fe macromolecules from diffusing towards crystalline sites. This leads to decreased crystallization growth rate. When the growth rate is comparable to nucleation rate, flower-like structures form. However, when more than enough amount of PPO is added, growth rate is decreased to a much lower level than nucleation rate. This leads to the formation of random aggregations. Thus, the optimized PPO amount must exist for the formation of flower-like structures,

where the decreased crystal growth rate is comparable to the nucleation rate.

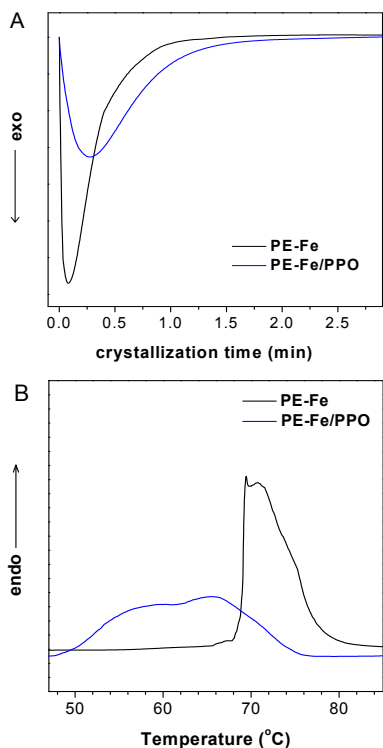


**Fig. 4** Heat flow traces during isothermal crystallization at 46 °C (A) and subsequent heating scan at a heating rate of 10 °C/min (B) of PE-Fe and PE-Fe/PPO in xylene, verifying crystallization of PE-Fe.

To check whether PPO remained in the flowers, FT-IR spectra of PE-Fe flowers were carried out, as shown in Fig. 5. The absorbance band at 2972  $\text{cm}^{-1}$  attributed to  $\text{CH}_3$  stretching vibration of PPO was absent in PE-Fe flowers, showing that PPO was not involved in PE-Fe flowers. PE-Fe flowers were further checked using  $^1\text{H}$  NMR. PE-Fe flowers suspended in deuterated DMSO were held at 120 °C for 10 min to disassemble PE-Fe flowers. Upon cooling to room temperature, PE-Fe/deuterated DMSO suspension was tested using  $^1\text{H}$  NMR. No PPO signals were detected, further verifying that PPO macromolecules were expelled out of PE-Fe flowers, although they played a crucial role during crystallization of PE-Fe. This was the possible reason why the addition of PPO did not decrease the degree of crystallinity of PE-Fe flowers.

#### Effect of polymeric dispersants

To further understand the mechanism of flower formation, we investigated the effect of polymeric dispersants on morphology of PE-PB particles. Hydrophilic poly(ethylene oxide) (PEO) and amphiphilic poly(ethylene oxide)-*b*-poly(propylene oxide)-*b*-poly(ethylene oxide) triblock copolymer (EPE) were also used as dispersants for the synthesis of PE-Fe particles under identical synthesis conditions. Not flowers, but large aggregates formed using PEO as dispersant (Fig. 6A). To exclude the effect of weight fraction and molecular weight of PEO, the weight ratio of PEO to PE-Fe ranging from 0.2:1 to 5:1 and molecular weight of

PEO in the range of 400 g/mol to 20000 g/mol were screened. No well-defined flowers were obtained. While flower-like structures with thin petals formed as using amphiphilic EPE as dispersant (Fig. 6B). It was apparent that hydrophobic PPO took more efficient effect on the formation of PE-PB flowers than hydrophilic PEO. The possible reason is that hydrophobic PPO is compatible with hydrophobic PE macromolecules at high temperature. During crystallization of PE-Fe, hydrophobic interaction between PPO and PE hinders the crystallization of PE-Fe to some extent. In contrast, weak interaction between hydrophilic PEO and hydrophobic PE takes an insignificant effect on the crystallization of PE-Fe.

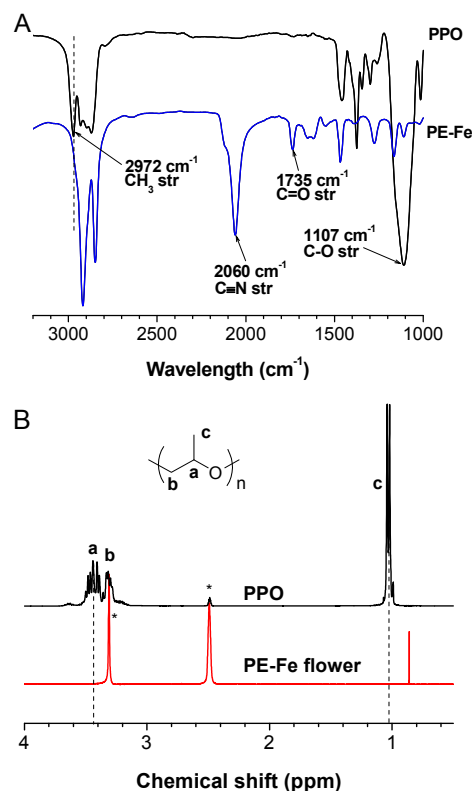


**Fig. 5** FT-IR (A) and  $^1\text{H}$  NMR (B) spectra of PPO and PE-Fe flowers showing the absence of PPO in PE-PB flowers. The solvent or water peak was denoted with asterisks.

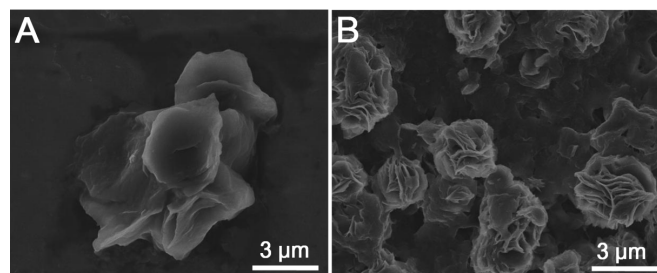


**Fig. 6** Typical scanning electron microscopy (SEM) images of PE-PB hybrid particles in the presence of PEO (A) and EPE triblock copolymer (B).

#### $\text{N}_2$ gas adsorption of PE-PB flowers

Fig. 7 shows the  $\text{N}_2$  gas adsorption and desorption isotherms of

PE-PB flowers and conventional PB particles. The amount of  $N_2$  gas adsorbed by PE-PB flowers was much larger than that by conventional PB particles in the range of  $P/P_0 = 0.1-1.0$ . This indicated that PE-PB flowers contained mesopores, which were fenced up by thin petals. BET surface of PE-PB flowers was  $152 \text{ m}^2/\text{g}$ , 3-fold of that of conventional PB particles ( $57.0 \text{ m}^2/\text{g}$ ). Moreover, a distinct hysteresis loop was observed for PE-PB flowers, assumably because that the hierarchical structures of flowers prevented  $N_2$  molecules adsorbed inside mesopores from releasing to some extent. Furthermore, PE-PB flowers showed the broad pore size distribution in a range of  $8 \text{ nm} - 60 \text{ nm}$  centred at  $10 \text{ nm}$ , which is close to the thickness of the petals of PE-PB flowers. The broad size distribution of mesopores is likely due to hierarchical structures of flowers.

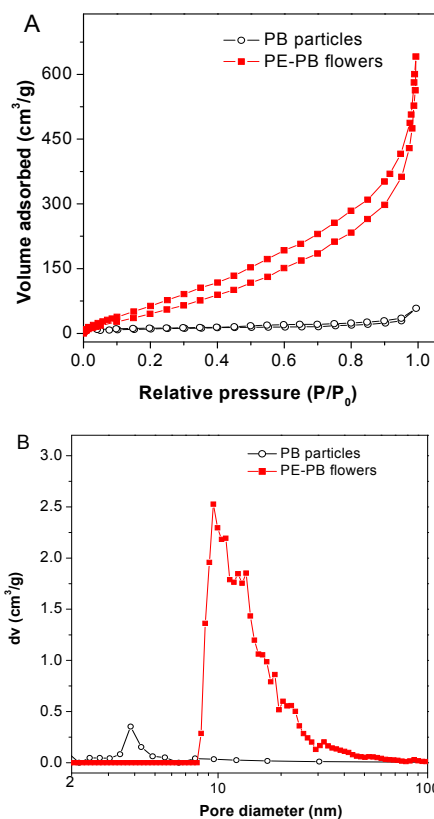


**Fig. 7** (A) Nitrogen gas adsorption and desorption isotherms obtained at  $77 \text{ K}$  and (B) pore size distribution plots for PE-PB flowers and conventional PB particles.

### Amperometric performance of PE-PB flowers

The electrochemical behaviour of PE-PB flowers was measured using cyclic voltammogram (CV). A typical CV curve of PE-PB flowers (Fig. 8) showed a distinct redox pair at  $E_{1/2} = 0.18 \text{ V}$ , ascribed to reversible Prussian white/Prussian blue conversion. We next tested the electrocatalytic activity of PE-PB flowers toward reduction of hydrogen peroxide ( $H_2O_2$ ). The electrodes decorated with PE-PB flowers showed good electrocatalytic activity, as shown in Fig. 8. The electrochemical reduction of hydrogen peroxide started at  $0.31 \text{ V}$ , positively shifting by  $0.10 \text{ V}$  contrasting to the bare electrode (Fig. S4). Such onset potential was close to that of the reduction of Prussian blue to Prussian

white, demonstrating that PE-PB flowers served as electron mediator for the reduction of hydrogen peroxide. Maximum reduction current of  $9.8 \mu\text{A}$  was obtained at  $0.16 \text{ V}$ , 3-fold of that for conventional PB particles (Fig. S5) under identical conditions, presumably related to the large surface area of PE-PB flowers. Cathodic current exhibited plateau at lower potentials.

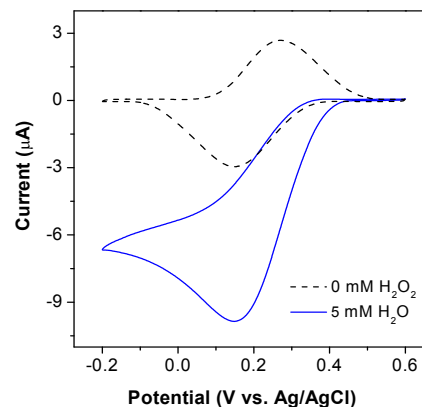


**Fig. 8** Cyclic voltammogram of PE-PB flowers deposited on glassy carbon electrodes in  $20 \text{ mM}$  phosphate buffer solution in the absence (dashed curves) and the presence of  $5 \text{ mM}$   $H_2O_2$  (solid curves). Scan rate:  $50 \text{ mV s}^{-1}$ , under  $N_2$ .

Current traces of PE-PB flowers and conventional PB particles upon stepwise addition of  $H_2O_2$  are shown in Fig. 9. Conventional PB particles showed small current response to hydrogen peroxide. In contrast, a two-fold current response to hydrogen peroxide was observed for PE-PB flowers. A detection limit of PE-PB flowers was determined to be  $22.5 \text{ nM}$ .

Finally, we tested the operation stability of sensors based on PE-PB flowers and conventional PB particles. The cathodic currents for reduction of  $H_2O_2$  as a function of time for PE-PB flowers and conventional PB particles were recorded (Fig. 10). The cathodic current of conventional PB particles decreased linearly with time. After  $2 \text{ h}$  conventional PB particles lost  $40 \%$  of their initial current. In contrast, PE-PB flowers remained  $80 \%$  of their initial current after  $2 \text{ h}$ , showing that PE-PB flowers showed enhanced electrochemical stability as contrast to conventional PB particles. A possible reason is that electrochemically active PB nanolayers are linked to inert polymer layers via covalent bonds, which prevents the labile Prussian white produced during the electrochemical reduction from leaking.

### Conclusions

In summary, we developed a facile and efficient approach for large-scale synthesis of organometallic PE-PB flowers with ultrathin petals. This approach involved crystallization of polyethylene capped with cyanoferrate complex in the presence of polymeric dispersants, followed by *in-situ* coordination polymerization of cyanoferrate complex with  $Fe^{3+}$ . The addition of proper amount of hydrophobic poly(propylene glycol) favoured the formation of flowers with thin petals contrasting to hydrophilic poly(ethylene glycol). PE-PB flowers showed enhanced surface area and improved electrocatalytic activity

towards reduction of hydrogen peroxide. Such crystallization induced hybrid flowers of organometallic polymers offer a catalogue of functional nanomaterials useful for bio-sensing, nano-devices and so on.

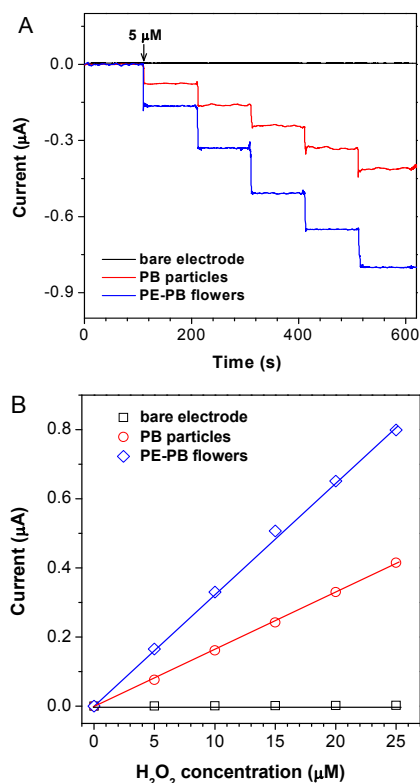


**Fig. 9** (A) Current traces of PE-PB flowers and conventional PB particles deposited on glassy carbon electrode upon stepwise addition of H<sub>2</sub>O<sub>2</sub> (5 μM each step) and (B) plots of current against H<sub>2</sub>O<sub>2</sub> concentration. Phosphate buffer solution (20 mM), pH: 7.4, under N<sub>2</sub>. Applied potential: 0.1 V.

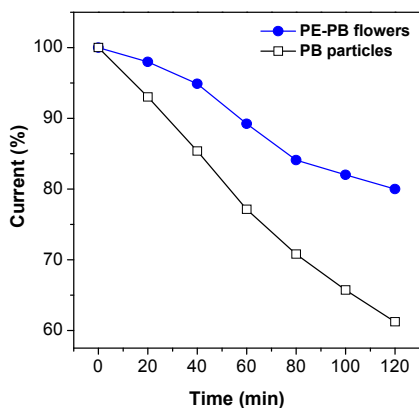


**Fig. 10** Long-term study of PE-PB flowers deposited on glassy carbon electrodes in 20 mM phosphate buffer solution in the presence of 5 mM H<sub>2</sub>O<sub>2</sub>. Applied potential: 0.1 V, under N<sub>2</sub>.

## Experimental

### Synthesis

To synthesize polymer/PB hybrid flowers, 10 mg semicrystalline polyethylene terminated with [Fe(II)(CN)<sub>5</sub>(4-(dimethylamino)-

pyridine)]Na<sub>2</sub>NH<sub>4</sub> (PE-Fe)<sup>32</sup> (scheme 1) and 10 mg poly(propylene oxide) (PPO) were dissolved in 5 mL *para*-xylene at 120 °C. The solution was held at 46 °C for 3 h, and then was allowed to restore to room temperature. The resulting suspension was added dropwise into 50 mL cold methanol with stirring, centrifuged and rinsed with methanol (50 mL × 3) to remove PPO. The solid was re-dispersed in 10 mL methanol with the assistance of sonication. To the suspension was added equivalent molar of Fe(NO<sub>3</sub>)<sub>3</sub> in 2 mL methanol with stirring. The resulting mixture was stirred overnight at room temperature. The mixture was centrifuged and top-layer solution was decanted. The solid was rinsed with methanol until the top-layer solution became colourless. The solid was dried in vacuum at 40 °C overnight to yield PE-PB hybrid flowers.

PB particles were prepared by slowly adding FeCl<sub>3</sub> aqueous solution (10 mL, 0.2 M) to pentacyano(4-(dimethylamino)pyridine)ferrate aqueous solution (10 mL, 0.2 M). The resulting suspension was stirred for 30 min at room temperature, followed by centrifugation and washing with distilled water 3 times. The resulting dark blue solid was collected by filtration and dried at 40 °C under reduced pressure.

### Characterization

FT-IR spectra were recorded using a Nicolet/Nexus 670 FT-IR spectrophotometer. Powder samples were mixed with KBr and then press into pellets for FT-IR measurements. Raman measurements were performed using a Renishaw inVia Raman spectrometer with a 633 nm excitation source. XPS spectra were recorded on a PHI-5600 multi-technique surface analysis system using a monochromatic Al K<sub>α</sub> X-ray source. A field-emission scanning electron microscope (SEM) (Hitachi S4800) was used to examine the morphologies of PE-PB hybrid flowers. The samples were mounted on freshly polished copper stoppers. The specimens were coated with a gold/platinum alloy thin film prior to observation. A field emission gun TEM microscope (JEM2010HR) equipped with an Oxford instruments UTW ISIS EDX system was used to characterize the microstructure of PE-PB hybrid flowers. Acceleration voltage was 200 kV. The sample was prepared by drying a drop of PE-PB/water suspension on a carbon-coated copper grid. The specimen was directly observed without staining due to the presence of iron elements. <sup>1</sup>H NMR spectra of polymers were carried out using Mercury-Plus 300 (VARIAN). DSC measurement was carried out using a Perkin-Elmer DSC-7 Instrument under nitrogen atmosphere. The temperature was calibrated with indium prior to the test. N<sub>2</sub> adsorption of PE-PB flowers were analyzed by means of an automated gas sorption analyzer (Autosorb-IQ C, Quantachrome, USA). The N<sub>2</sub> sorption isotherms were obtained by N<sub>2</sub> sorption at -196 °C (liquid nitrogen). Cyclic voltammetry was performed using a CHI-660D electrochemical analyzer (CH instruments, Inc.) in a three electrode cell. Glassy carbon working electrodes with a diameter of 3 mm were polished with slurry of 0.05 μm alumina particles, sonicated and rinsed with ultrapure water. After drying under N<sub>2</sub> flow, the glassy carbon working electrodes were made hydrophilic by treatment in oxygen plasma (1 Torr O<sub>2</sub>, 10 W) for 5 min. The cleaning process was repeated until no voltammetric features were observed between -0.2 - 1.2 V (vs Ag/AgCl) at the scan rate of 100 mV/s in 20 mM phosphate buffer solution. PE-PB flowers were dispersed in distilled water

with the assistance of sonication, and stored as a PE-PB hybrid flowers/water suspension at the concentration of 10 mg/mL. 3  $\mu$ L of PE-PB hybrid flowers/water suspension was deposited on freshly cleaned glassy carbon working electrodes. The solvent was allowed to evaporate at room temperature overnight. 20 mM phosphate solution was used as buffer solution. To remove oxygen, the buffer solution was degassed by bubbling N<sub>2</sub> for 40 min prior to CV measurements. Every sample was tested three times to obtain reproducible results.

## Acknowledgements

The financial support is from NSFC (21074151 and 21374136).

## Notes and references

DSAP lab, PCFM lab, GDHPPC lab, School of Chemistry and Chemical Engineering, Sun Yat-Sen University, Guangzhou 510275, China; E-mail: lgdong@mail.sysu.edu.cn

†Electronic Supplementary Information (ESI) available: SEM images of PE-PB particles at various PPO fractions, isothermal crystallization kinetics study of PE-Fe, amperometric performance of PB particles and bare electrodes. See DOI: 10.1039/b000000x/

- S. Husmann, E. Nossol and A. J. G. Zarbin, *Sensor Actuat. B-Chem.*, 2014, **192**, 782–790.
- S. Vaucher, J. Fielden, M. Li, E. Dujardin and S. Mann, *Nano Lett.*, 2002, **2**, 225–229.
- S. Vaucher, M. Li and S. Mann, *Angew. Chem. Int. Ed.*, 2000, **39**, 1793–1796.
- J. G. Moore, E. J. Lochner and A. E. Stieglman, *Angew. Chem. Int. Ed.*, 2007, **46**, 8653–8655.
- P. H. Zhou, D. S. Xue, H. Q. Luo and X. G. Chen, *Nano Lett.*, 2002, **2**, 845–847.
- M. Vondrova, T. M. McQueen, C. M. Burgess, D. M. Ho and A. B. Bocarsly, *J. Am. Chem. Soc.*, 2008, **130**, 5563–5572.
- R. S. Deshpande, S. L. Sharp-Goldman, J. L. Willson and A. B. Bocarsly, *Chem. Mater.*, 2003, **15**, 4239–4246.
- Z. D. Wang, J. Q. Zhang, J. M. Ekman, P. J. A. Kenis and Y. Lu, *Nano Lett.*, 2010, **10**, 1886–1891.
- H. L. Li, Y. Yang, Y. Z. Wang, W. Li, L. H. Bi and L. X. Wu, *Chem. Commun.*, 2010, **46**, 3750–3752.
- J. H. Kim, T. Kang, S. M. Yoo, S. Y. Lee, B. Kim and Y. K. Choi, *Nanotechnology*, 2009, **20**, 235302.
- Z. S. Yang, Z. H. Lin, C. Y. Tang and H. T. Chang, *Nanotechnology*, 2007, **18**, 255606.
- B. K. Jena and C. R. Raj, *Langmuir*, 2007, **23**, 4064–4070.
- L. Qian and X. R. Yang, *J. Phys. Chem. B*, 2006, **110**, 16672–16678.
- B. X. Wang, Y. C. Yin, C. J. Liu, S. S. Yu and K. Z. Chen, *Dalton T.*, 2013, **42**, 10042–10055.
- J. Zhou, G. H. Tian, Y. J. Chen, J. Q. Wang, X. R. Cao, Y. H. Shi, K. Pan and H. G. Fu, *Dalton T.*, 2013, **42**, 11242–11251.
- S. Y. Gao, Z. D. Li, K. Jiang, H. B. Zeng, L. Li, X. S. Fang, X. X. Jia and Y. L. Chen, *J. Mater. Chem.*, 2011, **21**, 7281–7288.
- M. Wolfs, T. Darmanin and F. Guittard, *Soft. Matter*, 2012, **8**, 9110–9114.
- Z. Y. Li, R. Liu, B. Y. Mai, S. Feng, Q. Wu, G. D. Liang, H. Y. Gao and F. M. Zhu, *Polym. Chem.*, 2013, **4**, 954–960.
- H. Qi, W. D. Wang and C. Y. Li, *ACS Macro Letters*, 2014, **3**, 675–678.
- L. Y. Li, C. Y. Li and C. Y. Ni, *J. Am. Chem. Soc.*, 2006, **128**, 1692–1699.
- G. D. Liang, L. T. Weng, J. W. Y. Lam, W. Qin and B. Tang, *ACS Macro Letters*, 2014, **3**, 21–25.
- R. M. Van Horn, J. X. Zheng, H. J. Sun, M. S. Hsiao, W. B. Zhang, X. H. Dong, J. T. Xu, E. L. Thomas, B. Lotz and S. Z. D. Cheng, *Macromolecules*, 2010, **43**, 6113–6119.
- W. N. He and J. T. Xu, *Prog. Polym. Sci.*, 2012, **37**, 1350–1400.
- G. D. Liang, J. T. Xu, Z. Q. Fan, S. M. Mai and A. J. Ryan, *Macromolecules*, 2006, **39**, 5471–5478.
- P. A. Rugar, L. Chabanne, M. A. Winnik and I. Manners, *Science*, 2012, **337**, 559–562.
- X. S. Wang, H. Wang, D. J. Frankowski, P. G. Lam, P. M. Welch, M. A. Winnik, J. Hartmann, I. Manners and R. J. Spontak, *Adv. Mater.*, 2007, **19**, 2279–2285.
- X. S. Wang, K. Liu, A. C. Arsenault, D. A. Rider, G. A. Ozin, M. A. Winnik and I. Manners, *J. Am. Chem. Soc.*, 2007, **129**, 5630–5639.
- X. S. Wang, G. Guerin, H. Wang, Y. S. Wang, I. Manners and M. A. Winnik, *Science*, 2007, **317**, 644–647.
- J. Schmelz, A. E. Schedl, C. Steinlein, I. Manners and H. Schmalz, *J. Am. Chem. Soc.*, 2012, **134**, 14217–14225.
- W. N. He, B. Zhou, J. T. Xu, B. Y. Du and Z. Q. Fan, *Macromolecules*, 2012, **45**, 9768–9778.
- W. N. He, J. T. Xu, B. Y. Du, Z. Q. Fan and F. L. Sun, *Macromol. Chem. Phys.*, 2012, **213**, 952–964.
- S. P. Bao, T. T. Liu, G. D. Liang, H. Y. Gao, F. M. Zhu and Q. Wu, *Chem. Eur. J.*, 2012, **18**, 15272–15276.
- Y. B. Liu and X. S. Wang, *Polym. Chem.*, 2012, **3**, 2632–2639.
- S. J. Ye, Y. B. Liu, S. J. Chen, S. Liang, R. McHale, N. Ghasdian, Y. Lu and X. S. Wang, *Chem. Commun.*, 2011, **47**, 6831–6833.
- R. McHale, Y. B. Liu, N. Ghasdian, N. S. Hondow, S. J. Ye, Y. Lu, R. Brydson and X. S. Wang, *Nanoscale*, 2011, **3**, 3685–3694.
- R. McHale, N. Ghasdian, Y. B. Liu, M. B. Ward, N. S. Hondow, H. H. Wang, Y. Q. Miao, R. Brydson and X. S. Wang, *Chem. Commun.*, 2010, **46**, 4574–4576.
- R. McHale, N. Ghasdian, Y. B. Liu, H. H. Wang, Y. Q. Miao and X. S. Wang, *Macromol. Rapid Commun.*, 2010, **31**, 856–860.
- G. D. Liang, J. T. Xu and X. S. Wang, *J. Am. Chem. Soc.*, 2009, **131**, 5378–5379.
- X. Roy, J. K. H. Hui, M. Rabnawaz, G. J. Liu and M. J. MacLachlan, *J. Am. Chem. Soc.*, 2011, **133**, 8420–8423.
- X. Roy, J. K. H. Hui, M. Rabnawaz, G. J. Liu and M. J. MacLachlan, *Angew. Chem. Int. Ed.*, 2011, **50**, 1597–1602.
- S. P. Bao, W. P. Qin, Q. H. Wu, G. D. Liang, F. M. Zhu and Q. Wu, *Dalton T.*, 2013, **42**, 5242–5246.
- M. Hu, S. Ishihara and Y. Yamauchi, *Angew. Chem. Int. Ed.*, 2013, **52**, 1235–1239.
- M. Hu, A. A. Belik, M. Imura and Y. Yamauchi, *J. Am. Chem. Soc.*, 2013, **135**, 384–391.
- M. Hu, J. Reboul, S. Furukawa, N. L. Torad, Q. M. Ji, P. Srinivasu, K. Ariga, S. Kitagawa and Y. Yamauchi, *J. Am. Chem. Soc.*, 2012, **134**, 2864–2867.
- M. Hu, S. Furukawa, R. Ohtani, H. Sukegawa, Y. Nemoto, J. Reboul, S. Kitagawa and Y. Yamauchi, *Angew. Chem. Int. Ed.*, 2012, **51**, 984–988.
- S. Z. Zhan, D. Guo, X. Y. Zhang, C. X. Du, Y. Zhu and R. N. Yang, *Inorg. Chim. Acta*, 2000, **298**, 57–62.
- L. Xia and R. L. McCreery, *J. Electrochem. Soc.*, 1999, **146**, 3696–3701.
- L. Chen, X. J. Wang, X. T. Zhang and H. M. Zhang, *J. Mater. Chem.*, 2012, **22**, 22090–22096.
- L. Xu, G. Q. Zhang, J. Chen, Y. F. Zhou, G. E. Yuan and F. L. Yang, *J. Power Sources*, 2013, **240**, 101–108.
- W. Chen, S. Cai, Q. Q. Ren, W. Wen and Y. D. Zhao, *Analyst*, 2012, **137**, 49–58.
- A. A. Karyakin, E. E. Karyakina and L. Gorton, *Electrochem. Commun.*, 1999, **1**, 78–82.